Mathematical modeling of 3-μm Erbium lasers

Şerban Georgescu

1. Introduction

Laser radiation at 3-μm is of great interest in medical and biological applications because water and hydroxyapatite, which are the major constituents of soft, and, respectively, hard (bones, tooth enamel) biological tissues, have very strong absorption in this region.

The most representative of 3-μm lasers is the erbium laser, working on the transition ${}^4I_{11/2} \rightarrow {}^4I_{13/2}$. A peculiarity of this transition is the "self-saturation": the lifetime of the terminal laser level is longer than the lifetime of the initial one. Despite this limitation, efficient long pulse or cw generation was obtained [1-12]. Various models have been proposed to explain the absence of the effects of the self-saturation. Basically, these models could be grouped in two classes, one based on the Excited State Absorption (ESA) from the terminal laser level [13-15] and the other based on energy transfer either to impurities or as a cooperative upconversion inside the Er^{3+} system [3, 16-19]. The presence of efficient laser emission in concentrated systems favors the last model. A direct experimental proof of the essential role of such an energy transfer mechanism as cooperative upconversion from ${}^4I_{13/2}$ was given in [20-22] for Er^{3+}: CaF_2 and Er^{3+}: YAG, where 3-μm stimulated emission was obtained for pumping in the terminal laser level.

In concentrated erbium systems, in addition to the upconversion from the terminal laser level, a large variety of other energy transfer processes, favored by the peculiar energy level scheme of Er^{3+}, could take place and could lower the efficiency of the driving upconversion mechanism. The main such mechanisms are: upconversion from the initial laser level ${}^4I_{11/2}$ [23], cross-relaxation from ${}^4S_{3/2}$ [24-26] and cross-relaxation from ${}^4I_{9/2}$ [27,28]. The upconversion from ${}^4I_{11/2}$ depletes the initial laser level, but its negative effect is partially attenuated by cross-relaxation from ${}^4S_{3/2}$ [18].

Based on the effective re-circulation of the excitation among the erbium levels, supraunitary quantum efficiency was predicted [23,29,30]. Till now, supraunitary quantum efficiency was experimentally demonstrated for several erbium doped crystals: Er: GSGG [7], Er: $YLiF_4$ [10], and Er: YAG [12].

The intrinsic limitations of the 3-μm erbium lasers, working in Q-switch regime, were discussed in [31]. Due to the specific mechanisms leading to the population inversion, only a limited fraction of the energy stored as a result of the optical pumping can be accessed during the giant laser pulse. The energy transfer mechanisms responsible for the high efficiency in long pulse or cw regime are too slow for tens-nanosecond Q-switch pulses.

Proceedings of The First French-Romanian Colloquium of Numerical Physics, October 30-31, 2000, Bucharest, Romania.

In order to understand how the 3-μm erbium lasers work, mathematical modeling proved to be a very valuable instrument [18, 29-34]. In the following, we shall try to explain the main properties of this laser system using a mathematical model, based exclusively on spectroscopic data, which includes the main energy transfer processes that take place in concentrated erbium doped crystals.

2. Generation on the Self-Saturated Er^{3+} Transition $^4I_{11/2} \rightarrow {}^4I_{11/2}$

2.1. Self-saturation condition

To explain the efficient 3-μm room-temperature laser on $^4\mathrm{I}_{11/2} \rightarrow {}^4\mathrm{I}_{11/2}$ transition we first discuss the "self-saturation condition". In fact, this condition is not $T_2 < T_1$ but $\alpha T_2 < \beta_{21}\beta T_1$, where α and β are the Boltzmann population coefficients of the Stark sublevels involved in the laser transition and β_{21} is the fraction of excitation from the initial laser level that reaches, radiatively or nonradiatively, the terminal laser level [35]. This self-saturation condition can be obtained by writing the rate equations for the laser levels in the absence of any energy transfer process:

$$\begin{aligned} \tfrac{dN_2}{dt} &= -\tfrac{N_2}{T_2} + R_{p2}N_0 \\ \tfrac{dN_1}{dt} &= -\tfrac{N_1}{T_1} + \beta_{21}\tfrac{N_2}{T_2} + R_{p1}N_0, \end{aligned} \tag{1}$$

where N_1 and N_2 are the populations of the final and initial laser levels; N_0 is the population of the ground level, $^4I_{15/2}$; and R_{pi} are the pump rates.

In the stationary regime, $dN_i/dt = 0$ and $N_2 = T_2 R_{p2} N_0$, $N_1 = \beta_{21}\left(R_{p1} + R_{p2}\right) N_0$. The condition for the population inversion between the Stark sublevels is $\alpha N_2 \geq \beta N_1$ i. e. $\alpha T_2 R_{p2} N_0 \geq \beta\beta_{21} T_1 \left(R_{p1} + R_{p2}\right) N_0$, which, in the case of the most convenient pumping conditions ($R_{p1} = 0$), becomes

$$\frac{T_2}{T_1} \geq \frac{\beta\beta_{21}}{\alpha} \tag{2}$$

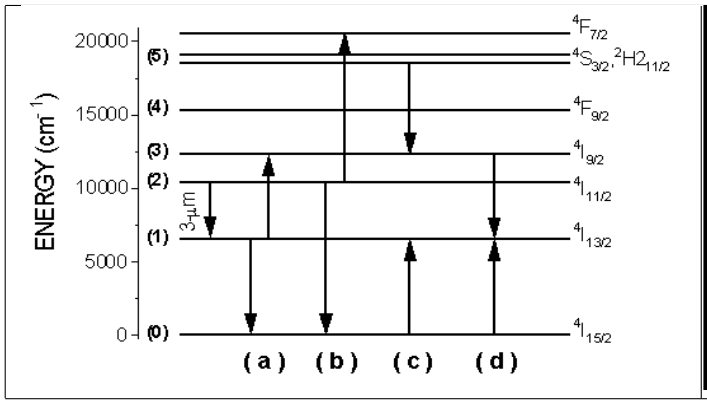

Fig. 1. Energy level scheme of Er^{3+} and the main energy transfer mechanisms: (a) upconversion from $^4I_{13/2}$, (b) upconversion from $^4I_{11/2}$, (c) cross-relaxation from $^4S_{3/2}$, and (d) cross-relaxation from $^4I_{9/2}$.

The possibility of fulfilling the condition of Eq. (2) depends of the specific transition (via the Boltzmann coefficients α and β and of the host crystal (T_1,T_2 and β_{21}). For example, the condition (2) can be fulfilled by the 2.81-μm transition of Er: $YLiF_4$ [36] ($\alpha = 0.201$, $\beta = 0.113$, $\beta_{21} \approx 0.6$, T_1= 10 ms and T_2= 4 ms (our measurements)), but for no transition in Er: YAG [37] (T_1= 6.4 ms, T_2= 0.1 ms). To explain the efficient cw (or long pulse) operation of the Er: YAG laser [3] cooperative upconversion or ESA from $^4I_{13/2}$ must be considered. Also, the effect of reducing the lifetime of the terminal laser level T_1 by codoping with ions as Tm^{3+} or Ho^{3+}, which seems to be beneficial from the condition (2), is examined in presence of the cooperative upconversion.

2.2. Cooperative upconversion

There are two main upconversion (two-ion) mechanisms acting in erbium systems at high concentrations:

Upconversion from $^4I_{13/2}$ [Fig. 1(a)]: ($^4I_{13/2} \rightarrow {}^4I_{15/2}$) + ($^4I_{13/2} \rightarrow {}^4I_{9/2}$), proposed by Bagdasarov et al. [3]. This "positive" mechanism takes out two excitations from $^4I_{13/2}$ and adds one to $^4I_{11/2}$ (via the efficient multiphonon transition $^4I_{9/2} \rightarrow {}^4I_{11/2}$).

Upconversion from $^4I_{11/2}$ [Fig. 1(b)]: ($^4I_{11/2} \rightarrow {}^4I_{15/2}$) + ($^4I_{11/2} \rightarrow {}^4F_{7/2}$), proposed in Ref. 23. This "negative" mechanism depletes the initial laser level.

Although the efficiency of a 3-μm depend on the rapport between the two upconversion mechanisms, significant for cw (or long pulse) generation is not the ratio ω_{22}/ω_{11}, where ω_{11} is the rate of the mechanism (1) and ω_{22} for mechanism (2), but the figure of merit $p \equiv (\beta/\alpha)\sqrt{\omega_{22}/\omega_{11}}$. In addition to these upconversion mechanisms, the rate equations describing the kinetics of the metastable levels of Er^{3+} include the cross-relaxation from $^4S_{3/2}$ [24-26] [Fig. 1 (c)] and the cross-relaxation from $^4I_{9/2}$ [27,28] [Fig. 1 (d)].

$$
\begin{aligned}
\tfrac{dN_5}{dt} &= -\left(a_{50}+a_{51}+a_{52}+a_{53}+a_{54}+w_{54}\right)N_5 - \omega_{50}N_5N_0 + \omega_{22}N_2^2 + R_{p5}N_0 \\
\tfrac{dN_4}{dt} &= -\left(a_{40}+a_{41}+a_{42}+a_{43}+w_{43}\right)N_4 + \left(a_{54}+w_{54}\right)N_5 + R_{p4}N_0 \\
\tfrac{dN_3}{dt} &= -\left(a_{30}+a_{31}+a_{32}+w_{32}\right)N_3 + a_{53}N_5 + \left(a_{43}+w_{43}\right)N_4 + \omega_{11}N_1^2 + \\
&\quad +\omega_{50}N_5N_0 - \omega_{30}N_3N_0 + R_{p3}N_0 \\
\tfrac{dN_2}{dt} &= -\left(a_{20}+a_{21}+w_{21}\right)N_2 + a_{52}N_5 + a_{42}N_4 + a_{32}N_3 - \\
&\quad -2\omega_{22}N_2^2 - \sigma\left(\alpha N_2 - \beta N_1\right)\phi + R_{p2}N_0 \\
\tfrac{dN_1}{dt} &= -a_{10}N_1 + a_{51}N_5 + a_{41}N_4 + a_{31}N_3 + \left(a_{21}+w_{21}\right)N_2 - 2\omega_{11}N_1^2 + \\
&\quad +\omega_{50}N_5N_0 + 2\omega_{30}N_3N_0 + \sigma\left(\alpha N_2 - \beta N_1\right)\phi + R_{p1}N_0 \\
\tfrac{d\phi}{dt} &= \tfrac{c\phi}{(n-1+l'/l)}\left[\sigma\left(\alpha N_2 - \beta N_1\right) - \rho\right] + k_{se}a_{21}N_2,
\end{aligned}
\tag{3}
$$

where N_0 to N_5 are the populations of $^4I_{15/2}$, $^4I_{13/2}$, $^4I_{11/2}$, $^4I_{9/2}$, $^4F_{9/2}$, and $^4S_{3/2}$ levels (thermalized, at room temperature, with $^2H2_{11/2}$). The coefficients $a_{ij}$and w_{ij} are the probabilities of radiative and, respectively, multiphonon ($i \rightarrow j$)

transitions. In the rate equations (3) the cross-relaxation processes are represented by ω_{50} (form $^4S_{3/2}$) and ω_{30} (from $^4I_{9/2}$). Pumping is allowed in any level i with the rate R_{pi}. In Eqs. (3) σ is the emission cross-section, c, the speed of light, ϕ, the photon density inside the laser resonator, and ρ, the total losses for a round trip. In the last of Eqs. (1) n represents the refraction index of the active medium of length l, l' is the length of the laser resonator and k_{se} is the proportionality coefficient for the fluorescence term which allows starting of the laser emission.

The radiative transition probability a_{ij} is the sum of the of electric- and magnetic-dipole probabilities.

$$a_{ij} = A_{ij}^{ed} + A_{ij}^{md} \tag{4}$$

The radiative lifetime is then given by

$$T_i^{rad} = \left(\sum a_{ij}\right)^{-1} \tag{5}$$

and probability of the multiphonon transition is

$$w_{ij} = \frac{1}{T_i^{fl}} - \frac{1}{T_i^{rad}} \tag{6}$$

where T_i^{fl} is the luminescence emission lifetime at very low Er concentration under weak resonant pump. The necessary spectroscopic data for Er: YAG, at room temperature, is given in Table 1.

Table 1. Spectroscopic data for Er: YAG, at room temperature.

Initial level	Terminal level	A_{ij}^{ed} (s^{-1})	A_{ij}^{md} (s^{-1})	T_i^{rad} (μs)	T_i^{fl} (μs)	w_{ij} (s^{-1})
$^4S_{3/2}$	$^4F_{9/2}$	0.6	-			
	$^4I_{9/2}$	60.5	-			
	$^4I_{11/2}$	31.8	-			
	$^4I_{13/2}$	446.6	-			
	$^4I_{15/2}$	1075.5	-	619	16	5.56×10^4
$^4F_{9/2}$	$^4I_{9/2}$	0.5	3.9			
	$^4I_{11/2}$	52.9	10.4			
	$^4I_{13/2}$	63.3	-			
	$^4I_{15/2}$	1485.7	-	629	1.5	6.65×10^5
$^4I_{9/2}$	$^4I_{11/2}$	0.6	1.5			
	$^4I_{13/2}$	45.9	-			
	$^4I_{15/2}$	178.3	-	4420	0.05	2×10^7
$^4I_{11/2}$	$^4I_{13/2}$	16.2	12.49			
	$^4I_{15/2}$	110.8	-	7170	100	9.86×10^3
$^4I_{13/2}$	$^4I_{15/2}$	97.9	56.3	6484	6500	$\sim$ 0

The electric-dipole transition probabilities A_{ij}^{ed} are calculated with the Judd-Ofelt model [38-40]. The magnetic-dipole transition probabilities (A_{ij}^{md}), between intermediary coupled states, were estimated with the expressions given in [41]. An inspection of Table 1 shows that for Er: YAG $w_{ij} >> a_{ij}$ except for $a_{10} >> w_{10}$. Therefore, we can consider that multiphonon transitions connect successive levels. In this case, the equation system (3) becomes

$$\begin{aligned}
\tfrac{dN_5}{dt} &= -\tfrac{N_5}{T_5} - \omega_{50}N_5N_0 + \omega_{22}N_2^2 + R_{p5}N_0 \\
\tfrac{dN_4}{dt} &= -\tfrac{N_4}{T_4} + \tfrac{N_5}{T_5} + R_{p4}N_0 \\
\tfrac{dN_3}{dt} &= -\tfrac{N_3}{T_3} + \tfrac{N_4}{T_4} + \omega_{11}N_1^2 + \omega_{50}N_5N_0 - \omega_{30}N_3N_0 + R_{p3}N_0 \\
\tfrac{dN_2}{dt} &= -\tfrac{N_2}{T_2} + \tfrac{N_3}{T_3} - 2\omega_{22}N_2^2 - \sigma\left(\alpha N_2 - \beta N_1\right)\phi + R_{p2}N_0 \\
\tfrac{dN_1}{dt} &= -\tfrac{N_1}{T_1} + \tfrac{N_2}{T_2} - 2\omega_{11}N_1^2 + \omega_{50}N_5N_0 + 2\omega_{30}N_3N_0 + \sigma\left(\alpha N_2 - \beta N_1\right)\phi + R_{p1}N_0 \\
\tfrac{d\phi}{dt} &= \tfrac{c\phi}{(n-1+l'/l)}\left[\sigma\left(\alpha N_2 - \beta N_1\right) - \rho\right] + k_{se}a_{21}N_2.
\end{aligned} \tag{7}$$

The cross-relaxation from ${}^4S_{3/2}$ plays a very important role in the structure of population of the laser levels. For moderate and high erbium concentrations, the excitation from this level, populated by direct pumping or by energy transfer, is equally distributed on the laser levels.

The effect of cross-relaxation from ${}^4I_{9/2}$, "inverse" to upconversion (1), is a reduction of the global efficiency and will be discussed later.

The rate equation system (7) can be further simplified if we take into account the inequality T_1, $T_2 >> T_3$, T_4, T_5, characteristic for the erbium system and the very efficient cross-relaxation from ${}^4S_{3/2}$. Assuming $\beta_{21} = 1$ (the case of Er: YAG [42]), over the laser threshold, in the stationary regime we have

$$\begin{aligned}
-\tfrac{N_2}{T_2} \quad & -\omega_{22}N_2^2 + \omega_{11}N_1^2 - \rho\phi + R_2N_0 = 0 \\
-\tfrac{N_1}{T_1} \quad & +\tfrac{N_2}{T_2} - 2\omega_{11}N_1^2 + \omega_{22}N_2^2 + \rho\phi + R_1N_0 = 0 \\
\alpha N_2 \quad & -\beta N_1 = \rho/\sigma,
\end{aligned} \tag{8}$$

where $R_1 = R_{p1} + R_{p5}$, $R_2 = R_{p2} + R_{p3} + R_{p4} + R_{p5}$.

The equation system (8) can be solved exactly for the populations N_1, N_2:

$$\begin{aligned}
N_1 &= \tfrac{-1+\sqrt{1+4\omega_{11}T_1^2(R_1+R_2)N_0}}{2\omega_{11}T_1}, \\
N_2 &= \tfrac{-1+\sqrt{1+4\omega_{22}T_2^2[(R_1+2R_2)N_0-N_1/T_1]}}{2\omega_{22}T_2}
\end{aligned} \tag{9}$$

For high pump intensities,

$$N_1 \approx \sqrt{\frac{\left(R_1+R_2\right)N_0}{\omega_{11}}}, \quad N_1 \approx \sqrt{\frac{\left(R_1+2R_2\right)N_0}{\omega_{22}}}. \tag{10}$$

The condition for population inversion, $\alpha N_2 - \beta N_1 > 0$, gives

$$\alpha N_2 - \beta N_1 \approx \alpha \sqrt{\frac{(R_1 + 2R_2)\, N_0}{\omega_{22}}} \left(1 - \frac{\beta}{\alpha} \sqrt{\frac{\omega_{22}}{\omega_{11}}} \sqrt{\frac{R_1 + R_2}{R_1 + 2R_2}} \right) > 0 \tag{11}$$

The last square root in Eq. (11) depends only on the pumping conditions (spectral composition of the pump radiation).

Eq. (11) suggests a figure of merit (formerly introduced in Ref. 43)

$$p \equiv \frac{\beta}{\alpha} \sqrt{\frac{\omega_{22}}{\omega_{11}}}, \tag{12}$$

which express the condition for population inversion

$$p \leq \sqrt{\frac{R_1 + 2R_2}{R_1 + R_2}} \tag{13}$$

The very interesting result is that now the condition for population inversion does not depend of the lifetime of the initial and terminal laser levels, overcoming the "bottleneck" produced by self-saturation.

The explicit effect of various parameters become apparent on examining the analytic expression of the photon flux density inside the laser resonator, obtained from Eqs. (8)

$$\begin{aligned} \phi \quad &= \tfrac{N_0}{\rho} \left[R_1 + (R_1 + R_2) \left(1 - p^2 \right) \right] - \tfrac{1}{\alpha \sigma T_2} \\ &- \tfrac{\omega_{22} \rho}{\alpha^2 \sigma^2} - \left(\tfrac{\beta}{\rho \alpha T_2} + \tfrac{2 \beta \omega_{22}}{\alpha^2 \sigma} \right) N_1 - \tfrac{1 - p^2}{\rho T_1}. \end{aligned} \tag{14}$$

Thus, only the first and the last terms on the right-hand side could be positive, depending on the pump rates and the figure of merit p [29,30,43]. The first term is positive if the condition (13) is satisfied; this gives $p < \sqrt{2}$ for $R_1 = 0$ (i. e. for pumping in one or all of the levels ${}^4F_{9/2}$, ${}^4I_{9/2}$ or ${}^4I_{11/2}$) and $p < 1$ for $R_2 = 0$ (pumping only in ${}^4I_{13/2}$). On the other hand, the last term in Eq. (14) is positive if $p < 1$ regardless the pump wavelength. The relative magnitude of these two terms restricts the possible combinations of the Stark sublevels of ${}^4I_{11/2}$ and ${}^4I_{13/2}$ for stationary laser emission for given pump conditions.

The lifetime T_2 of the initial laser level enters only in the denominator of the negative terms of Eq. (14) and should be as large as possible. The effect of the lifetime T_1 depends on p. If $p < 1$ the last term in Eq. (14) is negative and it is desirable to have large T_1; to the contrary, for $p > 1$ a shorter T_1 increases the photon flux density [44].

The upconversion parameter ω_{22} (from ${}^4I_{11/2}$) appears directly in two negative terms and indirectly in the figure of merit p. A small ω_{22} is always beneficial; it reduces the emission threshold and extends the range of the laser transitions.

The parameter ω_{11} influences the flux density by the intermediate of p and N_1. Generally, a large value of ω_{11} is beneficial. Nevertheless, for $p > 1$ there is a competition between the terms containing N_1; when $T_1/T_2 < (\alpha/\beta)\left(p^2-1\right)$, a lower value of ω_{11} may be preferred.

We can define the quantum efficiency of the 3-μm laser transition as the ratio between the number of quanta generated in the laser cavity and the number of pump quanta. The upper limit of the quantum efficiency for pumping performed in the level i is

$$\eta_i = \left[R_2 + (R_1+R_2)\left(1-p^2\right)\right]/R_{pi}. \tag{15}$$

Thus, for pumping in ${}^4S_{3/2}$, $\eta = 3-2p^2$, in ${}^4F_{9/2}$, ${}^4I_{9/2}$, or ${}^4I_{11/2}$, $\eta = 2-p^2$, and for pumping in ${}^4I_{13/2}$, $\eta = 1-p^2$. The result is that laser transitions with supraunitary quantum efficiency are possible. This is explained by the circulation of excitation specific to the erbium system.

2.3. ESA from ${}^4\boldsymbol{I}_{13/2}$

ESA from the terminal laser level ${}^4\mathrm{I}_{13/2}$ was considered as a possible mechanism for eliminating the self-saturation of the 3-μm erbium laser [13-15]. A noticeable ESA from ${}^4\mathrm{I}_{13/2}$ of the xenon lamp pump radiation was evident in Er: LuAG [14]. ESA cross-sections comparable with ground-sate absorption cross-section were measured in other crystals, too [45-49]. The effect of ESA on 3-μm emission depends strongly on the pump wavelength and can be taken into account by proper additional terms in the rate equations. If the pump wavelength $\lambda_p > 1.1\mu$m, ESA from ${}^4\mathrm{I}_{13/2}$ excites levels up to ${}^4\mathrm{F}_{9/2}$, avoiding the cross-relaxation from ${}^4\mathrm{S}_{3/2}$; however, for pump wavelength shorter than 0.85 μm, avoiding the cross-relaxation from ${}^4\mathrm{S}_{3/2}$ is activated. Denoting by R_{e1} the ESA pump rate for $\lambda_p > 1.1\mu$m and R_{e2} the ESA pump rate for $\lambda_p < 0.85\mu$m, the expression of the photon flux density becomes

$$\begin{aligned}\phi = {} & \tfrac{N_0}{\rho}\left[R_1 + (R_1+R_2)\left(1-p^2\right)\right] - \tfrac{1}{\alpha\sigma T_2} - \tfrac{\omega_{22}\rho}{\alpha^2\sigma^2} - \left(\tfrac{\beta}{\rho\alpha T_2} + \tfrac{2\beta\omega_{22}}{\alpha^2\sigma}\right)N_1 \\ & -\tfrac{1-p^2}{\rho T_1} + \tfrac{N_1}{\rho}\left[R_{e1} + \left(2-p^2\right)R_{e2}\right]\end{aligned} \tag{16}$$

Summing the first and the last terms in Eq. (16), we obtain the "pump term"

$$\psi = \frac{N_0}{\rho}\left[R_1 + (R_1+R_2)\left(1-p^2\right)\right] + \frac{N_1}{\rho}\left[R_{e1} + \left(2-p^2\right)R_{e2}\right] \tag{17}$$

The conditions imposed on p to have $\psi > 0$ are

1. For pumping in ${}^4I_{13/2}$, there is ESA to ${}^4I_{9/2}$ and $p^2 < 1 + \frac{R_{e1}N_1}{R_{p1}N_0}$.
2. For pumping in ${}^4I_{11/2}$, there is no ESA from ${}^4I_{13/2}$ and $p^2 < 2$.
3. For pumping in ${}^4I_{9/2}$ or ${}^4F_{9/2}$, whatever there is ESA from ${}^4I_{13/2}$ or not, $p^2 < 2$.
4. For pumping in ${}^4S_{3/2}$, there could be ESA from ${}^4I_{13/2}$ to ${}^2H2_{9/2}$ and

$$p^2 < 1 + \frac{1 + R_{e1}N_1/\left(R_{p4}N_0\right)}{1 + R_{e2}N_1/\left(2R_{p4}N_0\right)}.$$

The result is that ESA relaxes in some extent the condition on p when pumping is performed in ${}^4I_{13/2}$ or ${}^4S_{3/2}$.

To understand the possibilities of ESA by itself we consider that the only upconversion mechanism is ESA (the experimental situation of low erbium concentration). We consider two cases. In the first case, the pumping is performed in ${}^4S_{3/2}$. The rate equations in the stationary regime have the solutions

$$N_1 = \frac{\beta_{21} R_g N_0 T_1}{1 + (1 - \beta_{21}) R_{e2} T_1}, \quad N_2 = \frac{R_g N_0 T_2 (1 + R_{e2} T_1)}{1 + (1 - \beta_{21}) R_{e2} T_1}$$

where R_g is the rate of the pumping from the ground state ${}^4I_{15/2}$.

The condition for the population inversion gives

$$R_{e2} > -\frac{1}{T_2}\left(\frac{T_2}{T_1} - \frac{\beta_{21}\beta}{\alpha}\right) \tag{18}$$

The parenthesis in Eq. (18) becomes positive if the condition of Eq. (2) is satisfied; in this case (2.81-μm generation in $YLiF_4$) no ESA is necessary for the achievement of the population inversion. On the other hand, the presence of ESA could relax the condition (2). Thus, writing the inequality (18) in the form $\frac{\beta_{21}\beta}{\alpha} < \frac{T_2}{T_1} + R_{e2}T_2$, we see that higher values of the ratio β/α (i. e. shorter emission wavelengths) are permitted.

In the case of Er: YAG ($\beta_{21} \approx 1$, $R_{e1} > \frac{0.113}{0.201}\frac{1}{4000} = 6400$ μs, $T_2 = 100$ μs, $\beta/\alpha \approx 0.25$ for lasing at 2.94 μm) the condition (18) would require $R_{e1} > \frac{0.113}{0.201}\frac{1}{4000} \approx 2.3\times10^{-3}$ $\mu s^{-1} = 2300$ s^{-1}, a very high value (compared with a typical threshold value of ~ 5 s^{-1}. Therefore, in this case, only cooperative upconversion can overcome the "bottleneck" problem.

For pumping in ${}^4I_{13/2}$ the condition for population inversion becomes more drastic:

$$R_{e1} > \frac{\beta}{\alpha}\frac{1}{T_2} \tag{19}$$

This condition can be satisfied neither for Er: YAG nor for $YLiF_4$ (for $\lambda = 2.81$ μm, $R_{e1} > \frac{0.113}{0.201}\frac{1}{4000} \approx 1.4\times10^{-4}$ $\mu s^{-1} = 140$ s^{-1}, also, a too high value). Therefore, although ESA could improve the emission characteristics, it can not generally, solve by itself the self-saturation problem.

3. Figures of merit for 3-μm generation

Dimensionless figures of merit are very convenient to express the role of various energy transfer processes allowing the efficient generation of 3-μm erbium lasers. They permit a comparison of different materials candidate for laser emission and could furnish criteria for searching new materials. We could group these figures of merit in figures of merit significant for energy transfer processes, figures of merit related to presence of a sensitizer impurity, figures of merit related to the intrinsic oscillation threshold, and so on.

3.1. Figures of merit related to the upconversion processes

In the previous Section we introduced the dimensionless figure of merit p to express the role of the upconversion processes $p \equiv (\beta/\alpha)\sqrt{\omega_{22}/\omega_{11}}$. The importance of this figure of merit was discussed in details in the previous Section.

3.2. Figures of merit related to the cross-relaxation processes

Other dimensionless figures of merit can be introduced to express the influence of the cross-relaxation processes from ${}^4S_{3/2}$ and ${}^4I_{9/2}$.

If the level i is involved in a cross-relaxation process with the participation of the ground level ${}^4I_{15/2}$ (with the population N_0 assumed constant for low and moderate pump intensities) the kinetic equation for this level contains the terms

$$\frac{dN_i}{dT} = -\frac{N_i}{T_i} - \omega_{i0} N_0 N_i + \ldots = (1 + \omega_{i0} N_0 N_i)\,\frac{N_i}{T_i} + \ldots \tag{20}$$

We define the "efficiency" of the cross-relaxation process $i$as

$$e_i = \frac{\omega_{i0} N_0 T_i}{1 + \omega_{i0} N_0 T_i} < 1. \tag{21}$$

In this way we can introduce two figures of merit: e_5 for the cross-relaxation from ${}^4S_{3/2}$ and e_3 for the cross-relaxation from ${}^4I_{9/2}$. With these new figures of merit the rate equation system (8) becomes

$$\begin{array}{ll} -\frac{N_2}{T_2} & -(1+e_3)\,\omega_{22} N_2^2 + (1-e_3)\,\omega_{11} N_1^2 - \rho\phi + R_2 N_0 = 0 \\ -\frac{N_1}{T_1} & +\beta_{21}\frac{N_2}{T_2} - 2\,(1+e_3)\,\omega_{11} N_1^2 + (2e_3+e_5)\,\omega_{22} N_2^2 + \rho\phi + R_1 N_0 = 0 \\ \alpha N_2 & -\beta N_1 = \rho/\sigma. \end{array} \tag{22}$$

Usually, for moderate and high erbium concentrations, $e_5 \approx 1$ and the photon flux density becomes [28]

$$\begin{array}{l} \phi = \frac{R_p N_0}{\rho} - \frac{1}{\alpha\sigma T_2'} - \frac{\omega_{22}\rho}{\sigma^2\alpha^2}\frac{(1-e_3)}{1-e_3(1+p^2)} - \frac{N_1}{\rho}\left[\frac{\beta}{\alpha T_2'} + \frac{2\omega_{22}\beta\rho}{\sigma\alpha^2}\frac{(1-e_3)}{1-e_3(1+p^2)}\right] - \\ \quad -\frac{N_1}{\rho T_1}\frac{1-e_3-(1+e_3)p^2}{1-e_3(1+p^2)} \end{array} \tag{23}$$

where

$$\frac{1}{T_2'} = \frac{1}{T_2}\left\{1 + \frac{(1-\beta_{21})\left[1-e_3-(1+e_3)\,p^2\right]}{1-e_3\,(1+p^2)}\right\} \tag{24}$$

and the pump rate R_p has the expression

$$\begin{array}{l} R_p = \frac{R_{p1}\left[1-e_3+(1+e_3)p^2\right]+R_{p2}\left[2(1-e_3)-(1+2e_3)p^2\right]}{1-e_3(1+p^2)} + \\ \quad + \frac{(R_{p3}+R_{p4})\left[2(1-e_3)-(1+3e_3)p^2\right]+R_{p5}\left[3(1-e_3)-2(1+2e_3)p^2\right]}{1-e_3(1+p^2)} \end{array} \tag{25}$$

The high pump limit of the quantum efficiency for various pumping levels is given in Table 2. A general decrease of the quantum efficiency due to the cross-relaxation from $^4I_{9/2}$ is observed.

Table 2. Quantum efficiency (high pump limit) for pumping at different Er^{3+} levels.

Pumping level	Quantum efficiency η_i
$^4S_{3/2}$	$\frac{3(1-e_3)-2(1+2e_3)p^2}{1-e_3(1+p^2)}$
$^4S_{3/2}, ^4F_{9/2}$	$\frac{2(1-e_3)-(1+3e_3)p^2}{1-e_3(1+p^2)}$
$^4I_{11/2}$	$\frac{2(1-e_3)-(1+2e_3)p^2}{1-e_3(1+p^2)}$
$^4I_{13/2}$	$\frac{1-e_3-(1+3e_3)p^2}{1-e_3(1+p^2)}$

3.3. Figure of merit related to the presence of a sensitizer ion

Another figure of merit (denoted by f in Ref. 29) expresses the modification of the balance of rate equations due to the presence of the sensitizer Cr^{3+}. The position of the Cr^{3+} levels ^2E and $^4T_2$ in rapport with Er^{3+} levels favors the chain of processes $^4S_{3/2}$ (Er^{3+}) $\rightarrow$ ^2E, $^4T_2$ (Cr^{3+}) $\rightarrow$ $^4I_{9/2}$ (Er^{3+}), which furnishes an alternative channel for the de-excitation of $^4S_{3/2}$. In Ref. 29 this figure of merit was defined as

$$f = \frac{\omega_{50} N_{Er}}{\omega_{50} N_{Er} + \omega'_{50} N_{Cr}}, \tag{26}$$

where N_{Er} and N_{Cr} are, respectively, the chromium and erbium concentrations and ω'_{50} is the rate of the $Er^{3+} \rightarrow Cr^{3+}$ energy transfer process. Obviously, in the absence of chromium, $f = 1$.

In the presence of Cr^{3+} ions the analytical expression for the photon flux density becomes

$$\phi = \frac{R_{p3} N_0}{\rho} \frac{2(1-e_3) - p^2[(1-e_3)f + 4e_3]}{1-e_3+(1-f-e_3)p^2} - \frac{1}{\alpha\sigma T''_2} - \frac{\omega_{22}\rho}{\sigma^2\alpha^2} \frac{(1-e_3)(2-f)}{1-e_3+(1-f-e_3)p^2}$$
$$- \frac{N_1}{\rho}\left[\frac{\beta}{\alpha T_2^?} + \frac{2\omega_{22}\beta\rho}{\sigma\alpha^2} \frac{(1-e_3)(2-f)}{1-e_3+(1-f-e_3)p^2}\right] - \frac{N_1}{\rho T_1} \frac{1-e_3-(1+e_3)p^2}{1-e_3+(1-f-e_3)p^2} \tag{27}$$

where

$$\frac{1}{T_2''} = \frac{1}{T_2} \frac{1 + (1 - \beta_{21}) \left[1 - e_3 - (1 + e_3) p^2\right]}{1 - e_3 + (1 - f - e_3) p^2} \tag{28}$$

and the pumping is assumed only in the $^4I_{9/2}$ level with the rate R_{p3}. Only laser transitions that makes the first term (pumping term) positive are permitted. For $e_3 \neq 0$ the efficiency and the range of possible generation wavelengths are reduced. This loss could be compensated by the presence of Cr^{3+} (f ¡ 1), extending the emission toward shorter wavelengths.

3.4. Figures of merit related to oscillation threshold

3.4.1. Intrinsic oscillation threshold

In this section, we introduce new dimensionless figures of merit related to the oscillation threshold and we discuss the problem of the "intrinsic" oscillation threshold, characteristic for the 3-μm erbium lasers, working on a self-saturated transition. Since for this category of lasers the population inversion is created by the action of the upconversion mechanisms, the activation of these mechanisms costs an amount of pump energy (power), even in absence of any losses. We will denote this amount of energy (power) spent in the absence of any losses, as intrinsic oscillation threshold (IOT).

We have seen that for concentrated erbium crystals the condition (2) for population inversion is replaced by a qualitatively new condition (11). In this new condition does not enter the lifetimes of the laser levels and the self-saturation problem can be overcame. In this case, the relation between the material parameters ω_{11}, ω_{22} and the composition of the pumping light (i. e. the ratio of the pump rates R_1 and R_2) select the possible three-micron transition (represented by the Boltzmann population coefficients of the Stark sublevels involved in the laser transition, α and β).

In stationary conditions, the analytic expression of IOT is very simple. In terms of dimensionless quantities these expressions are

$$s_0 = \frac{2\tau \left(1 - p^2 + \tau\right)}{\left(1 - p^2\right)^2} \tag{29}$$

for pumping in $^4I_{13/2}$

$$s_0 = \frac{2 \left(\tau - 1\right) \left(1 - p^2 + \tau\right)}{\left(2 - p^2\right)^2} \tag{30}$$

for pumping in $^4I_{11/2}$, $^4I_{9/2}$, or $^4F_{9/2}$ and

$$s_0 = \frac{2 \left(\tau - \frac{1}{2}\right) \left(1 - p^2 + \tau\right)}{\left(3 - 2p^2\right)^2} \tag{31}$$

for pumping in $^4S_{3/2}$.

In Eqs. (29) we introduced new dimensionless figures of merit: dimensionless threshold

$$s_0 \equiv 2\omega_{11} T_1^2 R_p N_0 \tag{32}$$

and dimensionless lifetime

$$\tau \equiv \frac{\beta T_1}{\alpha T_2}. \tag{33}$$

Eqs. (29) to (31) allow a discussion about the IOT existence. For pumping in ${}^4I_{13/2}$ an IOT always exists (i. e. always $s_0 > 0$, Eq. (29)), regardless the host crystal. We note that, in given pumping conditions, $p < 1$. On the other hand, for pumping in ${}^4I_{11/2}$, ${}^4I_{9/2}$, or ${}^4F_{9/2}$ it is possible to have $s_0 < 0$ (no intrinsic threshold) if $\tau < 1$. This condition could be fulfilled for Er: $YLiF_4$ but not for Er: YAG. For Er: YAG ($T_1 = 6400 \quad \mu$s, $T_2 = 100 \quad \mu$s, $\alpha = 0.2$, and $\beta = 0.04$) $\quad \tau = 12.8 >> 1$. The condition $\tau < 1$ is equivalent with condition (2) with $\beta_{21} = 1$. In this case a population inversion can by built even for low concentrated crystals, where the effect of upconversion mechanisms is negligible. For pumping in ${}^4S_{3/2}$ the condition for the absence of IOT is even more restrictive: $\tau < 1/2$. We note than for Er: YAG crystals the IOT always exists, regardless the pumping conditions.

In the presence of losses, we can obtain an analytic expression for the oscillation threshold (OT). For pumping in ${}^4I_{13/2}$, using only dimensionless figures of merit, this expression is

$$\begin{aligned} s = s_0 \quad & + \tfrac{u}{1-p^2} + \tfrac{2t^2 + (t-u)\left(1-p^2-t+\tau\right)}{(1-p^2)^2} + \\ & + \tfrac{(t+\tau)\left(1-p^2+t+\tau\right)\sqrt{1+2u(1-p^2)/(t+\tau)^2}}{(1-p^2)^2} \end{aligned} \tag{34}$$

Similar expressions are obtained in the other pumping conditions.

In Eq. (34), we introduced supplementary figures of merit related to the presence of losses:

$$t \equiv \frac{2\omega_{22}\beta T_1}{\alpha^2}\frac{\rho}{\sigma} \text{ and } u \equiv 2\omega_{11} T_1^2 \left(\frac{\omega_{22}}{\alpha^2}\frac{\rho^2}{\sigma^2} + \frac{1}{\alpha T_2}\frac{\rho}{\sigma}\right). \tag{35}$$

3.4.2. Contribution of the intrinsic oscillation threshold to the oscillation threshold

We calculated the ratio s_0/s (i. e. the contribution of the intrinsic oscillation threshold to the oscillation threshold), function of erbium concentration as well as function of the total losses. The result of this calculation is presented in Fig. 2. We note a strong dependence of the IOT contribution function of both concentration and losses. For usual erbium concentrations (50%), the contribution of IOT is negligible, but for lower concentrates, the contribution of IOT could be important. The relative contribution of the IOT for two erbium concentrations (10% and 50%) is given in Table 3.

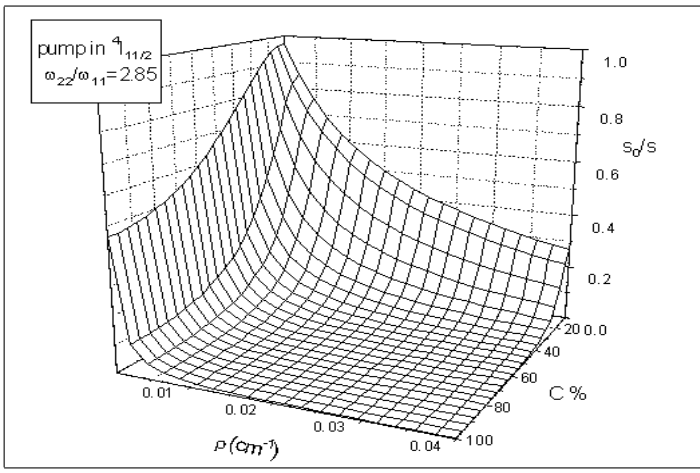

Fig. 2. Contribution of IOT to OT (s_0 / s) function of total losses and erbium concentration for Er: YAG laser, for pumping in $^4I_{11/2}$ ($^4I_{9/2}$ or $^4F_{9/2}$).

Table 3. The relative contribution of the intrinsic oscillation threshold to the total oscillation threshold in Er: YAG, for two erbium concentrations: 10% and 50%.

Pump level →	$^4I_{13/2}$	$^4I_{11/2}$ ($^4I_{9/2}$ or $^4F_{9/2}$).	$^4S_{3/2}$
Er (10%): YAG	s_0/s = 55%	s_0/s = 38.5 %	s_0/s = 46%
Er (50%): YAG	s_0/s = 4.2%	s_0/s = 2.5%	s_0/s = 3%

4. Stationary Regime

In this Section we resume the main aspects of the stationary regime of 3-μm erbium lasers. We have seen that the population inversion condition (2), expressed in terms of lifetimes of the laser levels, is replaced, in concentrated erbium systems by condition (11), expressed in terms of upconversion rates. This qualitative change is illustrated in Fig. 3. Pumping in the initial laser level is assumed. The slope of the dependence changes from $(\alpha T_2 - \beta T_1)\, N_0 < 0$, for low pump intensity, to $kR_2^{1/2} > 0$ (the proportionality coefficient k can be obtained from Eq. (11)). The oscillation threshold (OT) as well the intrinsic oscillation threshold (IOT) are shown for two erbium concentrations: 10% and 50%. For the higher concentration, both OT and IOT are significantly reduced. The losses are represented by the horizontal straight line marked ρ/σ.

The existence of the efficient energy transfer processes, recycling the excitation on the metastable levels of Er^{3+} make possible efficient stationary 3-μm generation, despite the unfavorable ratio of the lifetimes. The allowed ratio of the rates of the two

main two-ion upconversion processes (from $^4I_{11/2}$ - rate ω_{22} and from $^4I_{13/2}$ - rate ω_{11}) is given by the condition (11). This condition can be relaxed in some extent by ESA from $^4I_{13/2}$ (Eq. (16)) and by codoping with sensitizer ions as Cr^{3+} (Eq. (27)).

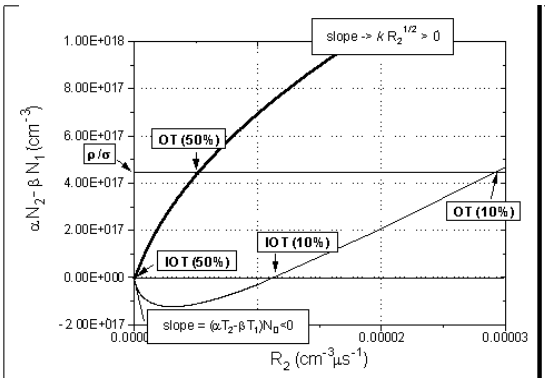

Fig. 3. Typical population inversion - pumping rate dependence for three-micron Er: YAG laser. The slope of the dependence changes from $(\alpha T_2 - \beta T_1)\, N_0 < 0$, for low pump intensity, to $kR_2^{1/2} > 0$. The oscillation threshold (OT) as well the intrinsic oscillation threshold (IOT) are shown for two erbium concentrations: 10% and 50%. For the higher concentration, both OT and IOT are significantly reduced. The losses are represented by the horizontal straight line marked ρ/σ.

The condition (11) (or (13)), though was obtained in stationary regime, is in fact, not restricted to this regime. This condition expresses the necessary requirements to overcome the "bottleneck" problem by recycling the excitation on the erbium levels.

In stationary regime we obtained simple analytical expressions for the photon flux density (Eqs. (14), (16), (23), and (27)). These expressions allowed a discussion of the role of various processes in the resulting characteristics of 3-μm erbium lasers and to find out the intrinsic limitations of these lasers. When possible, dimensionless figures of merit were introduced.

5. Q-Switch Regime

As we already mentioned in Section 1, 3-μm erbium lasers have many applications in medicine and biology. In surgery, in order to produce minimal thermal damage of the adjacent tissues in surgical operations, short pulses (if possible, in the nanosecond range) are desirable.

The Er: YAG laser, working in Q-switch regime at 2.94 μm (laser transition $^4I_{11/2} \rightarrow {}^4I_{13/2}$), could satisfy these requirements. Nevertheless, since this laser transition is self-saturated (i. e., the lifetime of the initial laser level is much shorter than the lifetime of the final one) efficient generation of short pulses is a quite delicate problem.

The generation of giant pulses of three-micron Erbium lasers was obtained experimentally, using different Q-switches such as spinning prism [50], electro-optic [51,52], passive [53, 54] and, more recently, FTIR (Frustrated Total Internal Reflection) [55-57].

There are few works devoted to the mathematical modeling of the Q-switching of three-micron Er-lasers, using a simplified two-level model, for which the initial

population inversion is taken from experiment (small signal, single pass amplification coefficient) [58]. Though the results of this modeling describe quite satisfactorily the experimental data, no connection was made between energy transfer processes governing three-micron lasing of Er laser, pumping conditions, co-doping, and the characteristics of giant pulse generation, as for cw emission [29,30].

In order to understand the peculiarities and the possibilities of the 3-μm Er lasers working in Q-switch regime, we construct and use a more general rate equation model, based exclusively on spectroscopic data, involving the populations of Er^{3+} energy levels up to $^4S_{3/2}$ and three energy transfer processes [31]: up-conversion from $^4I_{11/2}$ and $^4I_{13/2}$ and cross-relaxation from $^4S_{3/2}$. The necessary spectroscopic coefficients, entering the rate equations, were measured by us or were taken from literature. They are collected in Table 1 and Table 3. The simulations were performed using the rate equation system (3).

The Q-switch action was simulated for two cases: idealized (step function) and more realistic one, with 1.5 μs switching time, illustrating the FTIR device. The results of the simulations are then compared with data concerning the FTIR Q-switched Er: YAG lasers, for which more systematic experimental data are available in literature.

4.1. The FTIR Q-switch

Due to the rather low emission cross-section (Table 4) the pulse build-up time is long. Therefore, a Q-switch device, based on the FTIR phenomenon is a convenient choice. The construction of a FTIR Q-switch is schematically depicted in Fig. 4.

Table 4. Emission cross-section an energy transfer rates for Er (50 at. %): YAG

Parameter	Value	Reference
σ	2.6×10^{-20} cm^2	[59]
ω_{11}	1.3×10^{-15} cm^3 s^{-1}	[29]
ω_{22}	3.7×10^{-15} cm^3 s^{-1}	[29]
ω_{50}	1.06×10^{-15} cm^3 s^{-1}	[60]

Two prism (undoped YAG, highly transparent in 3-μm domain) are separated by a 1 μm foil. This separation, superior to the range of manifestation of the evanescent waves, assures total internal reflection of the laser radiation propagating along the resonator axis (low transmission state of the Q-switch). Applying a tension on the piezoelectric elements, the YAG prisms are deformed, the separation distance between the prism is reduced, and the transmission along the resonator axis increases substantially (high transmission state). In the following we shall simulate this Q-switch. Then, this Q-switch will be compared with an idealized one (step function).

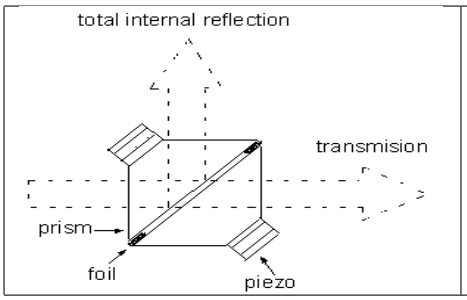

Fig. 4. Principle of the FTIR Q-switch. prism – undoped YAG prism; piezo – piezoelectric crystals.

The total loss per round trip, ρ, is expressed as

$$\rho = -\frac{\ln\left(r_1 r_2 T_Q^2\right)}{2l} + \rho_0 \tag{36}$$

where r_1, r_2 are the reflectivity of the total (rear) and partial (coupling) laser mirrors, T_Q is the one-way optical transmission of the Q-switch, and ρ_0 is the total passive loss coefficient.

The Q-switch operation is simulated in the Eqs. (3) changing the optical transmission of the Q-switch. This can be done assuming various temporal dependencies of transmission. The simplest case (idealized) is to consider a step function. However, we found that the change of the Q-switch transmission can be quite realistically represented by the expression

$$T_Q(t) = T_Q^{low} + \left(T_Q^{low} - T_Q^{high}\right)\left\{\left[\cos\left(\frac{2\pi}{\tau_Q}(t - t_1)\right)\right]^m - 1\right\} \tag{37}$$

where τ_Q and T_Q^{high} are, respectively, the values of the transmission in the closed and open state of the Q-switch and t_1 is the Q-switching moment. With two parameters τ_Q and m (where m is an even integer), we can control the fronts and the duration of the maximum transmission interval of the Q-switch. An example of the variation of the Q-switch transmission for τ_Q= 16 μs and m= 12, illustrating a FTIR Q-switch, is given in Fig. 5.

The energy of the giant pulse is calculated with the expression [61]

$$E_{pulse} = \frac{1}{2} h\, \nu_l\, A \ln\left(\frac{1}{2}\right) \int_{pulse} \phi(t) dt, \tag{38}$$

$h\nu_l$ being the energy of a laser photon and A the cross-section of the active element.

The FWHM (Full Width at Half Maximum) pulse-width, τ_{pulse}, is calculated in the so-called triangular approximation, i. e.

$$\tau_{pulse} = \frac{\int \phi(t)\, dt}{\phi_{\max}}, \tag{39}$$

where ϕ_{max} is the maximum value of the photon density.

4.2. Absorbed pump energy

In Eqs. (3) optical pumping is allowed in any level i with a pumping rate

$$R_{pi} = \frac{I_0 \sigma_{0i} \kappa_i}{h\nu_i}. \tag{40}$$

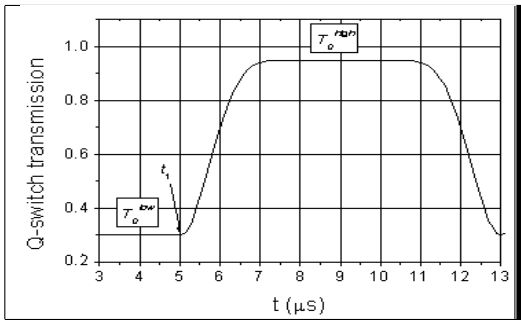

Fig. 5. Illustration of FTIR Q-switch transmission (Eq. (32)). $T_Q^{low} = 0.3$, $T_Q^{high} = 0.95$, $\tau_Q = 16$ μs, $m = 12$. Q-switching time, $t_Q \approx 1.5$ μs.

where I_0 is the incident power density, σ_{0i} is the maximal cross-section of the pump band i, $h\nu_i$ is the average pump quantum, and κ_i is the spectral pump coefficient i. e. the superposition integral of the spectral dependence $g(\lambda)$ of the pump source and the absorption cross-section, of Er^{3+} in YAG, with the spectral dependence $f(\lambda)$

$$\kappa_i = \int_{abs.band.i} g(\lambda) f(\lambda) d\lambda. \tag{41}$$

In case of monochromatic pump the distribution k_{p5} is much narrower than $f(\lambda)$ and the pumping wavelength is chosen to correspond to the maximum in the function $f(\lambda)$. However, in case of polychromatic pump (such as for flash lamp) we must take into account the contribution of the various pump bands. This can be done considering the normalized pump coefficients

$$k_{pi} = \frac{\sigma_{0i} \kappa_i}{\sum\limits_i \sigma_{0i} \kappa_i}. \tag{42}$$

The spectral distribution $f(\lambda)$ of the flash lamp is very complex; however, in order to get an idea on the contribution of the various pump levels for Er: YAG, we can approximate the flash lamp with a black body of 8000 - 12000 K, as in [62]. In Table 5 we give the calculated values of the normalized pumping coefficients k_{pi} for eleven absorption bands of Er^{3+} in YAG, for a 10000 K black body. It is evident that about 78 % of the pump energy are absorbed in the 0.355 - 0.565 μm spectral range. Due to the very rapid multiphonon relaxation of excitation from all the levels placed above $^4S_{3/2}$ on this last level, we can take $R_{p5} \approx 0.78 R(t)$ where $R(t)$ is the total pump rate of the system. The value of k_{p5} varies from 0.71 to 0.82 for black body temperatures from 8000 to 12000 K.

The total energy absorbed effectively by the Er: YAG crystal during the pump duration, Δt, in case of polychromatic pumping is given by

$$E_{abs} = \sum_{i=1}^{11} k_{pi} h\nu_i \int_0^{\Delta t} R(t)\, dt. \tag{43}$$

This equation assumes that the incident pump power density I_0 is the same in all the points of the sample. However, in the case of the strongly absorbing systems, such as concentrated Er crystals, marked departures from the uniform pump picture could take place.

Table 5. Spectral pumping coefficients of Er: YAG for pumping with Xenon flash lamp approximated with a black body with T = 10000 K.

Absorption transition	Wavelength range (μm)	k_{pi}
$^4I_{15/2} \rightarrow {}^4G_{9/2}, {}^2K_{15/2}$	0.355 – 0.375	0.1309
$^4I_{15/2} \rightarrow {}^4G_{11/2}$	0.375 – 0.390	0.2940
$^4I_{15/2} \rightarrow {}^2H_{9/2}$	0.400 – 0.420	0.0364
$^4I_{15/2} \rightarrow {}^4F_{3/2} + {}^4F_{5/2}$	0.435 – 0.465	0.0500
$^4I_{15/2} \rightarrow {}^4F_{7/2}$	0.480 - 0505	0.0970
$^4I_{15/2} \rightarrow {}^2H2_{11/2}$	0.515 – 0.540	0.1473
$^4I_{15/2} \rightarrow {}^4S_{3/2}$	0.540 – 0.565	0.0225
$^4I_{15/2} \rightarrow {}^4F_{9/2}$	0.640 – 0.680	0.1219
$^4I_{15/2} \rightarrow {}^4I_{9/2}$	0.780 – 0.860	0.0167
$^4I_{15/2} \rightarrow {}^4I_{11/2}$	0.940 – 1.030	0.0275
$^4I_{15/2} \rightarrow {}^4I_{13/2}$	1.440 – 1.580	0.0553

4.3. Losses of the absorbed energy

Not all the absorbed energy can be used in the laser emission: part of it is lost either non-radiatively by electron-phonon interaction (and this is transformed into heat) or in radiative processes.

4.3.1. Non-radiative losses

In crystals with high phonon energies (such as the oxides) the very efficient electron-phonon interaction leads to an almost complete non-radiative relaxation of excitation between close levels. Thus, as shown before, in case of the garnet crystals, almost all the energy absorbed in levels placed above $^4S_{3/2}$ relaxes non-radiatively on this level; in many of these crystals the level $^4I_{9/2}$ is quenched too. Because of this only a few well-separated levels could store the energy during the pump pulse (the levels 1 to 5 from Eqs. (3)). The fraction of pump energy lost by multiphonon relaxation from the levels above $^4S_{3/2}$ is given by

$$E_{nrad}^{(1)} = \sum_{i=6}^{11} k_{pi} h\nu_{i5} \int_0^{\Delta t} R\left(t\right) N_0\left(t\right) dt \tag{44}$$

where $h\nu_{i5}$ (with $i = 6$ to 11) correspond to the energy difference between the pump level and ${}^4S_{3/2}$ (pump quantum defects).

The energy stored in Er: YAG active medium is the sum of the potential energies stored in the five metastable levels 1 to 5. The non-uniform (Boltzmann) population of the Stark sub-levels imposes the definition of "thermal center of gravity" E_i^B:

$$E_i^B \equiv \sum_j E_{ij} \frac{\exp\left[-\left(E_{ij} - E_{i1}\right)/k_B T\right]}{\sum\limits_l \exp\left[-\left(E_{il} - E_{i1}\right)/k_B T\right]} \tag{45}$$

where E_{ij} is the j^{th} Stark sub-level of the level i, k_B is the Boltzmann constant, and T, the absolute temperature. The energy stored in a cm^3 of active medium at the moment of time t is

$$E_{stored}\left(t\right) = \sum_{i=1}^{5} N_i\left(t\right) h\nu_i^B. \tag{46}$$

Part of this stored energy can be lost during the time interval Δt by non-radiative processes, the main contribution coming from:

(*i*) the multiphonon relaxation from the metastable levels 1 to 5:

$$E_{nrad}^{(2)} = \int_0^{\Delta t} \left[\sum_{i=2}^{5} N_i\left(t\right) w_{i,i-1} h\nu_{i,i-1}\right] dt \tag{47}$$

(*ii*) the loss due to up-conversion processes ending above the level ${}^4S_{3/2}$: such a process is the co-operative up-conversion ω_{22} from level ${}^4I_{11/2}$ (labeled by 2 in our model) which ends up on the level ${}^4F_{7/2}$ (labeled by 6) from which it relaxes completely on ${}^4S_{3/2}$:

$$E_{nrad}^{(3)} = \int_0^{\Delta t} \omega_{22} N_2^2\left(t\right) h\nu_{65} dt. \tag{48}$$

(*iii*) the energetic balance of the energy transfer processes ending below ${}^4S_{3/2}$. Using the thermal centers of gravity, defined above, we have:

-an energy excess in the up-conversion from ${}^4I_{13/2}$:

$$\Delta E_e = 2 \times E_B\left({}^4I_{13/2}\right) - \left[E_B\left({}^4I_{9/2}\right) + E_B\left({}^4I_{15/2}\right)\right] \approx 778\mathrm{cm}^{-1}$$

which corresponds to generation of heat;

-an energy deficit in the cross-relaxation from ${}^4S_{3/2}$:

$$\Delta E_d = \left[E_B\left({}^4S_{3/2}\right) + E_B\left({}^4I_{15/2}\right)\right] - \left[E_B\left({}^4I_{9/2}\right) + E_B\left({}^4I_{13/2}\right)\right] \approx -533\text{cm}^{-1}$$

leading to an "absorption" of heat.

Thus, we can define another contribution to the non-radiative losses

$$E_{nrad}^{(4)} = \int_0^{\Delta t} \left[\omega_{11} N_1^2(t)\, h\nu_e - \omega_{50} N_0(t)\, N_5(t)\, h\nu_d\right] dt \tag{49}$$

where $h\nu_e$, $h\nu_d$, are, respectively, the excess and deficit energy per act.

The total main non-radiative losses (in J / cm^3) are thus

$$E_{nrad} = \sum_{k=1}^{4} E_{nrad}^{(k)}. \tag{50}$$

It is important to note that $E_{nrad}^{(1)}$ is included in the total losses only during the flash lamp pumping interval, while the other processes act also after the pump pulse.

4.3.2. Radiative losses

During the optical pumping and giant pulse generation a fraction of the absorbed energy is lost as spontaneous emission from the metastable levels. The energy lost by radiative transitions / cm^3 of active medium, during the optical pumping is

$$E_{rad} = \int_0^{\Delta t} \left\{ \sum_{i=1}^{5} N_i(t) \left[\sum_{j<i} a_{ij} h\nu_{ij} \right] \right\} dt \tag{51}$$

where a_{ij} and $h\nu_{ij}$ are related to the radiative transition $i \rightarrow j$; the same expression can be used for the radiative losses during the generation of the giant laser pulse.

4.4. Results of Q-switch simulation

4.4.1. Radiative and nonradiative losses during optical pumping

In our simulations we have used square pump pulses of various lengths, Δt. The Q-switch is open at the end of the pump pulse, when the maximal value of the population inversion is reached. Two types of Q-switches were considered: an idealized Q-switch, with the switching time t_Q= 0 (step function) and a FTIR Q-switch, with t_Q= 1.5 μs (see Fig. 5). In both cases, the maximum transmission was T_Q^{high}= 0.95. The effect of changing the maximum transmission can be included in ρ_0 (Eq. (36)) and a separate discussion of the influence of the passive losses on the emission characteristics will be presented bellow. The spectral composition of the pumping light was either monochromatic or corresponding to a black body with absolute temperature T = 10000 K. For square pumping pulses we could consider that the variations of

temperature, and, as a consequence, the change of the spectral composition of the emission of the flash lamp are not important.

The radiative losses / cm^3, as well the non-radiative ones (heat), produced during the optical pumping, function of the absorbed energy are presented in Fig. 6a and Fig. 6b, respectively, for monochromatic and flash lamp pumping. For the pump pulse length we have chosen the usual value $\Delta t = 200$ μs [55,56]. For flash lamp pumping, the non-radiative losses, due to the multiphonon relaxation of the high Er^{3+} energy levels on $^4S_{3/2}$, $E^{(1)}_{nrad}$, were included. We see that the radiative losses are negligible in rapport with the non-radiative ones. Obviously, the losses during the optical pumping are larger for longer pump pulse lengths, and, therefore, shorter pump pulses are preferable. Only small changes in the dependence of the non-radiative losses in rapport with the spectral composition of the pumping light are noted (Fig. 6b). The radiative losses are inferior to 0.08 % of the absorbed energy.

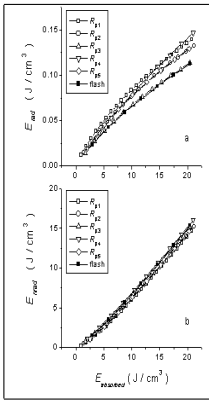

Fig. 6. Radiative and non-radiative losses (in J / cm^3) function of absorbed energy, for monochromatic and flash lamp (approximated by a 10000 K black body) pumping: a - radiative losses; b - non-radiative losses. The radiative losses can be neglected in rapport with non-radiative ones.

4.4.2. Stored energy

Regardless the pumping wavelengths, all the energy levels of Er^{3+}, from $^4I_{13/2}$ up to $^4S_{3/2}$, are populated during the optical pumping. In this model the contribution of higher energy levels of Er^{3+} in YAG, as for example, $^2P_{3/2}$, are not taken into account, though, up-conversion processes, which can populate this level, were experimentally evidenced [64]. In fact, at high Erbium concentration the luminescence of $^2P_{3/2}$ level is strongly quenched, but the cross-relaxation mechanisms are not yet clear. Therefore, we will use for the stored energy (in J / cm^3) Eq. (46). Due to the radiative and non-radiative losses, the energy storage efficiency (i. e., the ratio between the stored and absorbed energy) depends of the intensity and duration of the pumping pulse. We show this dependence in Fig. 7, where the total absorbed energy / pumping pulse was kept constant (= 20 J /cm^3). The energy storage efficiency is higher for shorter pumping pulses. For example, for $\Delta t = 100$ μs, this efficiency is ~ 33 %, but becomes only ~ 15 %, for $\Delta t = 500$ μs. In experiment the pumping pulse duration is limited by the constructive characteristics of the flash lamps, the laser threshold for the Er: YAG laser being quite high. We must note that in this simulation the change of the

color temperature of the flash lamp plasma for higher current densities, required by short pumping pulses, was not taken into account.

4.4.3. Giant pulse generation

The FTIR Q-switch proved to be a convenient solution for three-micron Er lasers, mainly due to the lower voltage required in rapport with the conventional Pockels cells. Therefore, in our calculations we shall simulate the Q-switch function by changing the Q-switch transmission according to Eq. (37), with T_Q^{low}= 0.30, T_Q^{high}= 0.95 and a Q-switching time of 1.5 μs (see Fig. 5), that corresponds to the FTIR device described in Ref. [55,56]. The Q-switch is opened at the end of the pumping pulse, when the population inversion, for square pump pulses, reaches its maximum. The results are then compared with an idealized situation, with the Q-switching time t_Q= 0 (step function). If not specified otherwise, we will consider the following parameters: pumping (flash lamp) 200 μs square pulse, a volume of the active medium (Er (50 at. %): YAG) of 1 cm^3, with length l = 8 cm and cross-section A = 0.125 cm^2 (as used in Ref. 56), and a resonator length, l' = 27 cm. The mirrors reflectivity is R_1 = 1 (rear mirror) and R_2 = 0.78 (coupling mirror), and the passive loss coefficient is, ρ_0= 0 cm^{-1}. For an active medium of 8 cm length, the value of the transmission T_Q^{high}= 0.95 corresponds to ρ_0= 0.0064 cm^{-1}.

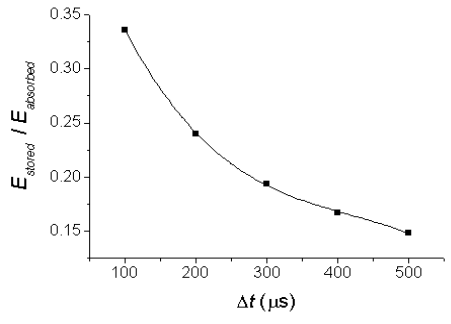

Fig. 7. Efficiency of the energy storage in the active medium function of the pumping pulse duration (flash lamp pumping, square pulses). The pumping rate, $R(t)$ was chosen to have the same absorbed energy (in our example, 20 J / cm^3) for various pumping pulse duration (100, 200, 300, 400, and 500 μs). The continuous solid line represents a fitting with a third degree polynom.

4.4.3.1. Q-switch efficiency.

Two different approaches were used in calculating the energy generated during the giant laser pulse: (*i*) with Eq. (38), (*ii*) considering the variation of the stored energy in the active medium (Eq. (46)) during the giant laser pulse and subtracting the radiative and non-radiative losses. We must note that the losses produced during the giant pulse can not be neglected, especially near laser threshold. An illustration of input-output characteristics is given in Fig. 8 for the FTIR Q-switch.

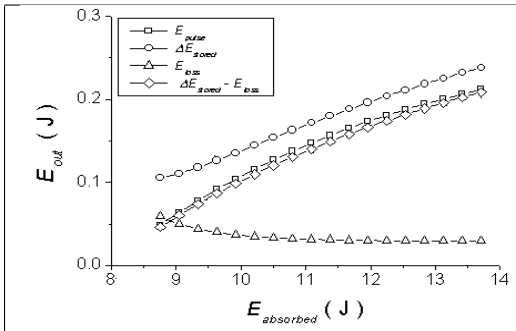

Fig. 8. Input - output characteristics for a FTIR Q-switch with $T_Q^{high} = 0.95$, switching time t_Q= 1.5 μs. The active medium has 1 cm^3 volume (l = 8 cm, A = 0.125 cm^2). The resonator length is l' = 27 cm and the mirrors reflectivity are, respectively, R_1 = 1, R_2 = 0.78. E_{pulse} - giant pulse energy calculated with Eq. (6); ΔE_{stored} - variation of the total stored energy (Eq. (14)) during the giant pulse generation; E_{loss} - total (radiative and non-radiative) losses.

A comparison between the FTIR and the idealized Q-switch, for various resonator lengths, is given in Fig. 9. The rather good performances of the FTIR Q-switch, especially for longer resonators, are explained by the low value of the emission cross-section leading to long build-up times (function of the resonator length, the build-up time could vary between 0.5 an 2 μs). For both FTIR and idealized Q-switches, shorter resonators lead to lower laser thresholds and lower efficiencies. A "saturation" of the efficiency is observed for long resonators.

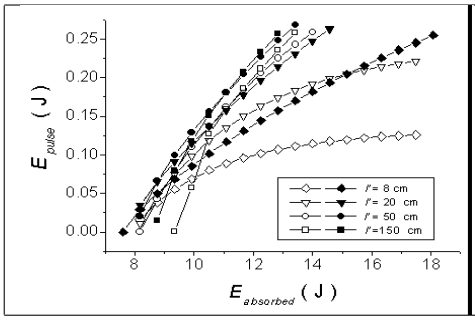

Fig. 9. Comparison between the output characteristics of FTIR (open symbols) and the idealized (solid symbols) Q-switches, for various lengths of the laser resonator, l'. Due to a long pulse build-up time the efficiency difference between the FTIR and the idealized Q-switches is not drastic, especially for long resonators.

The influence of the spectral composition of the pumping light on the emission characteristics is shown in Fig. 10. Two types of pumping were simulated: monochromatic pumping in any of the levels $^4I_{13/2}$, $^4I_{11/2}$, $^4I_{9/2}$, $^4F_{9/2}$, and $^4S_{3/2}$ and flash lamp pumping (approximated by a 10000 K black body). The emission efficiency for monochromatic pumping respects the same trends as for cw emission [29], i. e. the highest efficiency is obtained for pumping in the initial laser level and the lowest for pumping in the terminal one. The even lower efficiency in the case of flash lamp pumping is explained by the multiphonon degradation of the energy absorbed in the bands situated at higher energies than $^4S_{3/2}$. The influence of the passive losses on the emission efficiency is given in Fig. 11

4.4.3.2. Pulse-width.

The FWHM pulse-width, τ_{pulse}, was calculated with Eq. (39). Generally, for shorter resonator lengths, shorter giant pulses and higher peak power values are obtained. As shown in Fig. 12, the dependence τ_{pulse} versus E_{pulse} is practically independent of the spectral composition and the pump efficiency, i. e. the parameters usually less known in experiment. Furthermore, this dependence is very sensitive to the total passive losses (Fig. 13) and to the resonator length (Fig. 14). Therefore, this type of dependence could be very convenient to compare the experimental and theoretical results.

4.4. Discussion concerning the results of Q-switch simulation

For usual pumping pulses duration (200 - 300 μs, for Er: YAG Q-switched laser) we could consider the levels populations close to the stationary values, especially for high pump intensities. On the other hand, our analysis shows that thought the role of the energy transfer processes is essential for the realization of the population inversion, their influence on the evolution of populations, during the giant pulse generation, can be neglected. Thus, the problem of Q-switching Er: YAG lasers can be separated into two distinct moments: (i) the construction of the population inversion during the optical pumping, when the energy transfer mechanisms are essential; (ii) the giant pulse generation, when the evolution of the photon density inside the laser resonator takes place practically independent of the existence of these energy transfer processes. Therefore, for not very short pumping pulses, within a rather good approximation, some of the main conclusion of the cw regime [29] could be applied to the Q-switch regime. Thus, the efficiency should be highest for pumping in the initial laser level, $^4I_{11/2}$ and lowest for pumping in the terminal laser level, $^4I_{13/2}$, as confirmed by the present calculations (Fig. 10). We note that for shorter pumping pulses ($\leq$ 100 μs), the inverse of the rates of the energy transfer processes are comparable with pumping pulses duration: $(\omega_{11}N_1)^{-1} \approx (1.3 \text{ x } 10^{-21} \text{ cm}^3 \ \mu\text{s}^{-1} \text{ x } 10^{19} \text{ cm}^3)^{-1} = 77$ μs, $(\omega_{22}N_2)^{-1} \approx (3.7 \text{ x } 10^{-21} \text{ cm}^3 \ \mu\text{s}^{-1} \text{ x } 10^{19} \text{ cm}^3)^{-1} = 27$ μs, where, near the laser threshold, $N_1 \approx N_2 \approx 10^{19}$ cm^3. In this case the populations could be far from the stationary values and the conclusions of the cw theory could be not longer valid.

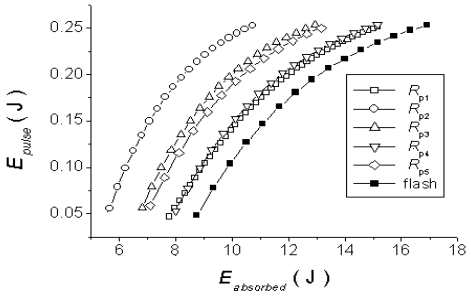

Fig. 10. Influence of the spectral composition of the pumping light on the efficiency of giant pulse generation (FTIR Q-switch). As for cw Erbium lasers, the highest efficiency is obtained for pumping in the initial laser level, $^4I_{11/2}$. The lowest efficiency, obtained for flash lamp pumping, is explained by degradation in heat of the pumping energy absorbed in Er^{3+} energy levels, higher than $^4S_{3/2}$.

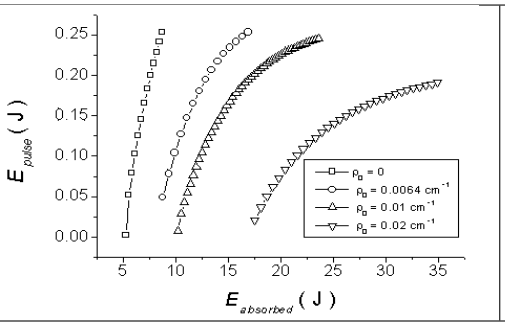

Fig. 11. Output characteristics of the Er: YAG laser (FTIR Q-switch) function of the passive losses, ρ_0, for T_Q^{high}= 1. The value ρ_0 = 0.0064 cm^{-1} represents the losses induced by T_Q^{high}= 0.95.

As pointed in [29], the 2.94 μm laser transition of Er in YAG, for long pumping pulses or stationary pumping, is characterized by a subunitary figure of merit $p = (\beta/\alpha)\sqrt{(\omega_{22}/\omega_{11})}$= 0.43. In this case, the value of the terminal laser level lifetime, T_1, should be kept as large as possible for efficient lasing [44]. For the Q-switch regime our simulations show the same tendency: the reduction of T_1, though could help the formation of the laser pulse, it reduces the population inversion and the overall result is negative. On the contrary, for transitions with $p > 1$, the reduction of T_1 is twice beneficial: it improves the population inversion and helps the formation of the giant pulse. This improvement is illustrated in Fig. 15 by simulating the Q-switching the Cr: Er: YAG (co-doped with Ho^{3+} or Tm^{3+}) laser, working on the 2.70 μm transition ($\alpha \approx 0.25$, $\beta \approx 0.27$, $p = 1.85$), with an emission cross-section, $\sigma \sim 7.5$ x 10^{-20} cm^2, as estimated from the published fluorescence spectra [62]. We note that, according to the mathematical model for cw regime [29], laser transitions with $p > \sqrt{2}$ are made possible by co-doping with ions as Cr^{3+}, which introduce a concurrent de-excitation channel for $^4S_{3/2}$, that changes the mechanisms of population inversion. Thus, in Ref. 29, the presence of Cr^{3+} ions is marked in the rate equations by a supplementary figure of merit $f \equiv \omega_{50}N_0N_5/(\omega_{50}N_0N_5 + \omega'_{50}N_{Cr}N_5)$ where ω'_{50} is the rate of the supplementary de-excitation channel and N_{Cr} is the concentration of the Cr^{3+} ions. In the absence of Cr^{3+} ions, $f = 1$. An inspection of the rate equations (3) shows that the presence of Chromium changes the term $\omega_{50}N_0N_5$ to $\omega_{50}N_0N_5/f$ only in the first and the third of Eqs. (3), but preserves it unchanged in the fifth one. In our example (depicted in Fig. 15 for the idealized, step function, Q-switch) we have chosen $f = 0.1$. The strong reduction of the lifetime of the terminal laser level, $^4I_{13/2}$, will result, eventually, to a normal four level laser system. We note that in this case, the depletion of the $^4I_{13/2}$ population by transfer to impurities introduces a new source of non-radiative losses, not considered in Eq. (50). Furthermore, the depletion of the $^4I_{13/2}$ population should reduce the overall emission efficiency in rapport with the case when the energy stored in the $^4I_{13/2}$ level is re-cycled by up-conversion (e. g., 2.94 μm emission). This is illustrated in Fig. 15: the 2.94 μm emission (shown with solid symbols) has an efficiency slope significantly higher, for the same laser configuration, than the 2.7 μm one.

In contrast with the radiative losses, the non-radiative ones constitute an important factor in degrading the energy stored in the active medium. We found that

for 200 μs flash lamp pulses, 50÷70 % of the absorbed energy is transformed into heat. We note that both up-conversion mechanisms, from $^4I_{13/2}$ and $^4I_{11/2}$, being followed by rapid multiphonon relaxation, which make them practically irreversible, are important sources of heating. Besides, another important source of heating is the multiphonon transition $^4I_{11/2} \quad \sim> \ ^4I_{13/2}$. Recently [65], the experimental study of the heating of Er: YAG active medium during optical pumping was used as an alternative method to the spectroscopic and laser ones, to check the rate equations models and the published spectroscopic data.

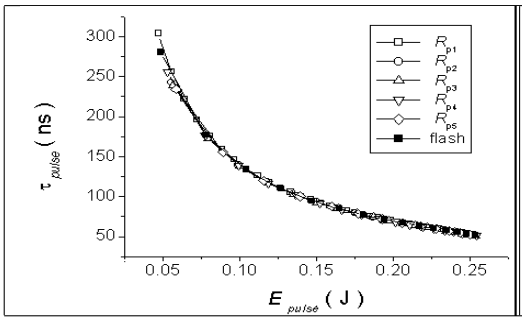

Fig. 12. FHWM pulse-width, τ_{pulse}, versus pulse energy, E_{pulse}, for various spectral compositions of the pumping light (FTIR Q-switch).

In our model the complex Stark level structure was simplified to those of the thermal centers of gravity. In this simplified model the energy transfer processes appear as off resonant. (An analysis of these energy transfer processes shows that resonance is assured by transitions between particular pairs of Stark sublevels). We took into account these off-resonances by introducing a new term, $E^{(4)}_{nrad}$ in the non-radiative losses.

A rather unexpected result is that non-radiative losses are not negligible, even during the generation of giant laser pulses. Near the laser threshold the variation of the stored energy leads almost entirely to heat. A comparison of the results of our analysis for the 2.94 μm FTIR Q-switched emission of Er: YAG laser with published experimental data [55,56] show that the theory presented here gives a good qualitative description of these data. However, generally, the experimental giant pulses are less energetic that this mathematical model predicts. Using the FHWM pulse-width, τ_{pulse}, versus pulse energy, E_{pulse}, representation, giant pulses with energy less than 100 mJ and shorter than 100 ns, for comparable laser configurations and active media, can be obtained only for passive losses $\rho_0 > 0.02$ cm^{-1}. Taking into account the very strong absorption of the water at 2.94 μm, water vapor traces present in the atmosphere could introduce, for long resonators, rather high passive losses. On the other hand, the rate equation model requires a population inversion at the laser threshold, significantly higher than the experimental value (estimated to approx. 1.2x10^{18} cm^3, from Ref. [56]). Therefore, to explain the discrepancy between the experiment and theory we should look for the possible non-uniformity of the population inversion inside the active medium, resulting in a non-homogeneous distribution of the emission intensity across the emitting surface of the laser rod. In fact, hot spots in the near

field image of the Er: YAG emission have been observed, even when special attention was paid to assure very uniform pumping conditions. This non-uniformity could be equivalent with a reduction of the effective emitting surface area.

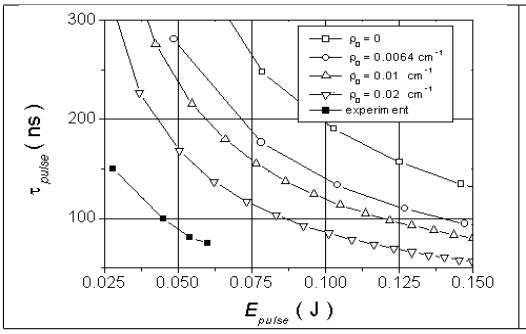

Fig. 13. τ_{pulse} versus E_{pulse}, curves for various passive losses, ρ_0 (FTIR Q-switch, $l' = 27$ cm, $T_Q^{high} = 0.95$). The full symbols represent experimental results obtained in a comparable laser configuration [55].

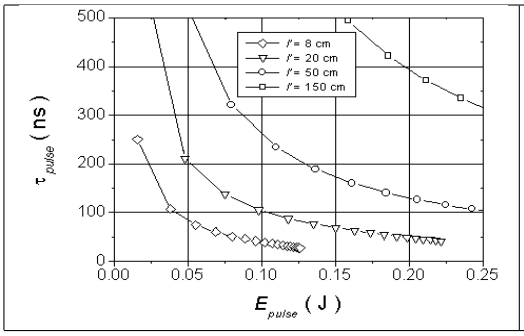

Fig. 14. τ_{pulse} versus E_{pulse} curves for various resonator lengths l' (FTIR Q-switch, $T_Q^{high} = 0.95$, $\rho_0 = 0$).

A major cause for non-uniform distribution of the population inversion could be the non-uniform pump intensity due to the strong absorption in concentrated Er systems; this effect could be accentuated by non-uniform heating of the active medium under pump. Also, under certain wavelengths of pumping, the excited state absorption could influence the populations of the excited levels.

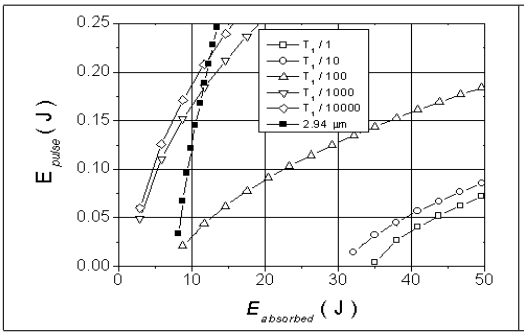

Fig. 15. Influence of the reduction of the terminal level lifetime, T_1, for a 2.7 μm Cr: Er: YAG laser output (open symbols). For comparison, with solid symbols, is given the 2.94 μm emission characteristic, in a similar laser configuration.

5. Conclusion

Efficient 3-μm generation of erbium lasers on the self-saturated transition $^4I_{11/2} \rightarrow {}^4I_{13/2}$ is made possible by energy transfer processes that are very active at high activator concentrations. The population inversion condition, which depends at low erbium concentrations of the lifetimes of the laser levels and can be fulfilled in only a few cases (as, for example, 2.81-μm lasing in Er: $YLiF_4$) is replaced at higher concentrations by a new one, that depends only of the upconversion rates.

For the stationary regime of emission, our mathematical model, based on analytical formulae for population inversion, photon flux density, and quantum efficiency, explains in an unitary manner the main characteristics of erbium lasers.

The role of various interactions that influence 3-μm lasing in erbium systems is expressed by appropriate dimensionless figures of merit that can be determined from spectroscopic measurements. Our rate equation model can also accommodate the presence of sensitizer ions, represented by specific figure of merit. These figures of merit can be used as criteria for searching new materials for 3-μm generation.

The same mathematical model was used for simulation of the Q-switch regime of 3-μm erbium lasers. The FTIR Q-switch, though characterized by microsecond switching times, proves to be very convenient for 2.94-μm Er: YAG lasers due to the rather long pulse build-time. For usual pump duration (200-300 μs) the main conclusions for the stationary regime are still valid. Thus, for the construction of the population inversion the energy transfer mechanisms are essential, but during the giant pulse generation these processes are "frozen". This fact leads to major limitation of the efficiency of the 3-μm erbium lasers in Q-switch regime.

References

[1] Kh. S. Bagdasarov, V. A. Lobachev, and T. M. Murina, "Study of generation characteristics of YAG: Er^{3+} laser ($\lambda = 2.94$ μm) under pulsed pump of millisecond duration," *Proc. 5^{th} All-Union Conf., Optics of Lasers,* Leningrad, 1987, S. E. Vavilov Ed., State Instit. Opt., p. 247 (in Russian).

[2] M. A. Andriasyan, N. V. Vardanyan, and R. B. Kostanyan, "Millisecond $Lu_3Al_5O_{12}$:Er laser," *Sov. J. Quantum Electron.,* **12**, 366-369 (1982).

[3] Kh. S. Bagdasarov, V. I. Zhekov, V. A. Lobachev, T. M. Murina, and A. M. Prokhorov, "Steady-state emission from a $Y_3Al_5O_{12}$:Er^{3+} laser ($\lambda = 2.94$ μm, T=300 $^\circ$K)," *Sov. J. Quantum Electron.*, **13**, 262-263 (1983).

[4] G. J. Kinz, R. Allen, L. Esterowitz, "cw and pulsed 2.8 μm laser emission from diode-pumped Er^{3+}: $LiYF_4$ and room temperature," *Appl. Phys. Lett.*, **50**, 1553-1555 (1987).

[5] P. Al'bers, V. G. Ostroumov, A. F. Umyscov, S. Schnell, and I. A. Shcherbakov, "Low threshold YSGG:Cr:Er laser for the 3-μm range with a high pulse repetition frequency," *Sov. J. Quantum Electron.,* **18**, 558-559 (1988).

[6] S. Wüthrich, W. Lüthy, and H. P. Weber, "Comparison of YAG: Er and $YalO_3$: Er laser crystals emitting near 2.9 μm," *J. Appl. Phys.,* **68**, 6467-5471, (1990).

[7] R. C. Stoneman, L. Esterowitz, "Efficient resonantly pumped 2.8-μm GSGG laser," *Opt. Lett.*, 17, 816-818, (1992).

[8] B. Schmaul, G. Huber, R. Clausen, B. Chai, P. LiKamWa, M. Bass, "Er^{3+}: $YLiF_4$ continuous wave cascade laser operation at 1620 and 2810 nm at room temperature," *Appl. Phys. Lett.*, **62**, 541-543 (1993).

[9] B. J. Dinerman, P. F. Moulton, "3-μm cw laser operations in erbium-doped YSGG, GGG, and YAG," *Opt. Lett.*, **19**, 1143-1145, (1994).

[10] T. Jenssen, A. Diening, G. Huber, "Investigation of diode-pumped 2.8-μm Er: $LiYF_4$ lasers with various doping levels," *Opt. Lett.*, **21**, 585-587, (1996).

[11] M. Tikerpae, S. D. Jackson, T. A. King, "2.8 μm Er: YLF laser transversely pumped with a CW diode laser bar," *Opt. Commun.*, **167**, 283-290 (1999).

[12] Da-Wun Chen, C. L. Fincher, T. S. Rose, F. L. Vernon, R. A. Fields, "Diode-pumped 1-W continuous-wave Er: YAG 3-μm laser," *Opt. Lett.*, **24**, 385-387 (1999).

[13] M. A. Andriasyan, N. D. Vardanyan, and R. B. Kostanyan, "Influence of the absorption of the excitation energy from the $^4I_{13/2}$ level of erbium ions on the operation of $Lu_3Al_5O_{12}$:Er crystal lasers," *Sov. J. Quantum Electron.,* **12**, 804-806 (1982).

[14] G. K. Demirkhanyan, S. M. Harutyunyan, R. B. Kostanyan, T. B. Sanamyan, and F. P. Safaryan, "Investigations of absorption from the laser level $^4I_{13/2}$ of the erbium ions in the lutetium garnet," *Opt. Commun.*, **59**, 49-51 (1986).

[15] S. Hubert, D. Meichenin, B. V. Zhou, and F. Auzel, "Emission properties, oscillator strengths and laser parameters of Er^{3+} in $LiYF_4$," *J. Lumin.*, **50**, 7-15 (1991).

[16] A. A. Kaminskii, T. I. Butaeva, A. O. Ivanov, I. V. Mochalov, A. G. Petrosyan, G. I. Rogov, and V. A. Fedorov, "New data on stimulated emission of crystals containing Er^{3+} and Ho^{3+} ions," *Sov. Tech. Phys. Lett.*, **2**, 308-310, (1976).

[17] V. I. Zhekov, V. A. Lobachev, T. M. Murina, and A. M. Prokhorov, "Cooperative phenomena in yttrium erbium aluminum garnet crystals," *Sov. J. Quantum Electron.*, **14**, 128-130 (1984).

[18] S. Georgescu, V. Lupei, I. Ursu, V. I. Zhekov, V. A. Lobachev, T. M. Murina, and A. M. Prokhorov, "The role of cross-relaxation mechanisms in the quasistationary generation regime of YAG: Er laser," *Rev. Roum. Phys.*, **31**, 857-864 (1986).

[19] V. I. Zhekov, T. M. Murina, A. M. Prokhorov, M. I. Studenikin, S. Georgescu, V. Lupei and I. Ursu, "Cooperative processes in $Y_3Al_5O_{12}$-Er^{3+} crystals," *Sov. J. Quantum Electron.*, **16**, 274-276 (1986).

[20] S. A. Pollack, D. B. Chang, and N. L. Moise, "Up-conversion pumped infrared erbium lasers," *J. Appl. Phys.*, **60**, 4077-4086 (1986).

[21] V. I. Zhekov, V. A. Lobachev, T. M. Murina, A. V. Popov, A. M. Prokhorov, and M. I. Studenikin, "Lasing in $Y_3Al_5O_{12}$: Er^{3+} ($\lambda = 2.94$ μm) crystals as a result of selective excitation of the lower active level," *Sov. J. Quantum Electron.*, **19**, 737-738 (1989).

[22] P. Xie and S. C. Rand, "Continuous-wave, pair-pumped laser," *Opt. Lett.*, **15**, 848-850 (1990).

[23] Kh. S. Bagdasarov, V. I. Zhekov, V. A. Lobachev, A. A. Manenkov, T. M. Murina, and A. M. Prokhorov,. "Cross-relaxation YAG: Er^{3+} laser," *Izv. ANSSSR,* ser. fiz., **48**, 1765-1770 (1984).

[24] L. G. Van Uitert and L. F. Johnson, "Energy transfer between rare-earth ions," *J. Chem. Phys.*, **44**, 3514-3522 (1966).

[25] A. Lupei, V. Lupei, S. Georgescu, I. Ursu, V. I. Zhekov, T. M. Murina, and A. M. Prokhorov, "Many-body energy processes between Er^{3+} ions in yttrium aluminum garnet," *Phys. Rev. B.*, **41**, 10923-10932 (1990).

[26] V. I. Zhekov, T. M. Murina, A. M. Prokhorov, M. I. Studenikin, S. Georgescu, A. Lupei, and V. Lupei, "Nonradiative transfer of excitation energy in crystals with the interaction of three-optically active centers," *JETP Lett.*, **52**, 670-674 (1990).

[27] H. Chou and H. P. Jenssen, "Up-conversion processes in Er-activated solid state laser materials," *Tunable Solid State lasers,* Eds. M. L. Shand and H. P. Jenssen, vol. 5, pp. 167-174, OSA Proc. Series, 1989

[28] S. Georgescu, T. J. Glynn, R. Sherlock, and V. Lupei, "Concentration quenching of the $^4I_{9/2}$ level of Er^{3+} in laser crystals," *Optics Commun.*, **106**, 75-78 (1994).

[29] V. Lupei, S. Georgescu, and V. Florea, "On the dynamics of population inversion for 3 μm Er^{3+} lasers," *IEEE J Quantum Electron.*, **29**, 426-434 (1993).

[30] V. Lupei and S. Georgescu, "Erbium three-micron laser emission as an up-conversion system", *Opt. Eng.*, **35**, 1265-1272, (1996).

[31] S. Georgescu and V. Lupei, "Q-switch regime of 3-μm Er: YAG lasers," *IEEE J. Quantum Electron.*, **34**, 1031-1040 (1998).

[32] A. M. Prokhorov, V. I. Zhekov, T. M. Murina, N. N. Platnov, "Pulsed YAG: Er^{3+} laser efficiency (analysis of model equations)," *Laser Physics*, **3**, 79-83 (1993).

[33] M. Pollnau, Th. Graf, J. E. Balmer, W. Lüthy, H. P. Weber, "Explanation of the cw operation of the Er^{3+} 3-μm crystal laser,", *Phys. Rev. A*, **49**, 3990-3996 (1994).

[34] M. Pollnau, R. Spring, S. Wittwer, W. Lüthy, H. P. Weber, "Investigations on the slope efficiency of a pulsed 2.8-μm Er^{3+} $LiYF_4$ laser," *J. Opt. Soc. Am. B*, **14**, 974-978 (1997).

[35] R. S. Quimby and W. J. Miniscalco, "Continuous-wave lasing on a self-terminating transition," *Appl. Optics*, **28**, 14-16 (1989).

[36] S. Hubert, D. Meichenin, B. V. Zhou, F. Auzel, "Emission properties, oscillator strengths and laser parameters of Er^{3+} in $LiYF_4$," *J. Lumin.*, **50**, 7-15 (1991).

[37] S. Georgescu, V. Lupei, A. Lupei, V. I. Zhekov T. M. Murina, M. I. Sudenikin, "Concentration effects on the up-conversion from the $^4I_{13/2}$ level of Er^{3+} in YAG," *Opt. Commun.*, **81**, 186-192 (1991).

[38] B. R. Judd, "Optical absorption intensities of rare-earth ions," *Phys. Rev.*, **127**, 750-755 (1962).

[39] G. S. Ofelt, "Intensities of crystal spectra of rare-earth ions," *J. Chem. Phys.*, **37**, 511-520 (1962).

[40] S. Georgescu, C. Ionescu, I. Voicu, and V. I. Zhekov, "A modified Judd-Ofelt analysis of Er^{3+} in YAG," *Rev. Roum. Phys.*, **30**, 265-276 (1985).

[41] B. G. Wybourne*, Spectroscopic Properties Of Rare Earths*, J. Wiley & Sons, 1965.

[42] S. Georgescu a, V. Lupei, T. J. Glynn, R. J. Sherlock, "Intensity pump effects in the kinetics of $^4I_{11/2}$ level in ErAG," *Opt. Commun.*, **155**, 61–67 (1998).

[43] M. A. Noginov, S. G. Semenkov, V. A. Smirnov, I. A. Shcherbakov, "Effect of interaction between excited erbium ions on the formation of inverse population on the $^4I_{11/2} \rightarrow {}^4I_{13/2}$ transition in a YAG: Cr, Er crystal under stationary excitation," *Opt. Spektrosk.*, **69**, 120-127 (1990).

[44] V. Lupei, S. Georgescu, V. Florea, "The effect of terminal laser level lifetime on three-micron laser emission in Er-doped crystals," *Opt. Commun.*, **92**, 67-72 (1992).

[45] P. Le Boulanger, J. -L. Doualan, S. Girard, J. Margerie, and R. Moncorgé, "Excited-state absorption spectroscopy of Er^{3+} -doped $Y_3Al_5O_{12}$, YVO_4, and phosphate glass," *Phys. Rev. B*, **60**, 11380-11390 (1999).

[46] J. Koetke and G. Huber, *Appl. Phys. B: Lasers Opt.*, "Infrared excited-state absorption and stimulated-emission cross sections of Er^{3+} -doped crystals,"**61**, 151-158 (1995).

[47] Y. Guyot, H. Manaa, J. Y. Rivoire, R. Moncorgé, N. Garnier, E. Descroix, M. Bon, and P. Laporte, "Excited-state-absorption and upconversion studies of Nd^{3+} doped single crystals $Y_3Al_5O_{12}$, $YLiF_4$, and $LaMgAl_{11}O_{19}$," *Phys. Rev. B*, **51**, 784-799 (1995).

[48] M. Pollnau, E. Heumann, T. Danger, and G. Huber, "Experimental determination of radiative-transition rates and quantum efficiencies in Er^{3+}: $YAlO_3$," *Opt. Commun.*, **118**, 250-254 (1995).

[49] P. Le Boulanger, J. -L. Doualan, S. Girard, J. Margerie, R. Moncorgé, and B. Viana, "Excited-state absorption of Er^{3+} in the $Ca_2Al_2SiO_7$ laser crystal," *J. Lumin.*, **86**, 15-21 (2000).

[50] Kh. S. Bagdasarov, V. I. Zhekov, L. A. Kulevskii, V. A. Lobachev, T. M. Murina, and A. M. Prokhorov, "Giant laser radiation pulses from erbium-doped yttrium aluminum garnet," *Sov. J. Quantum Electron.*, **10**, 1127-1131 (1980).

[51] E. V. Zharikov, N. N. Il'ichev, S. P. Kalitin, V. V. Laptev, A. A. Malyutin, V. V. Osiko, P. P. Pashinin, A. M. Prokhorov, Z. S. Saidov, V. A. Smirnov, A. F. Umyskov, and I. A. Shcherbakov, "Spectral, luminescence, and lasing properties of a yttrium scandium gallium crystal activated with chromium and erbium," *Sov. J. Quantum Electron.*, **16**, 635-639 (1986).

[52] J. Breguet, A. F. Umyskov, W. Lüthy, I. A. Shcherbakov, and H. P. Weber, "Electro-optically Q-switched 2.79 μm YSGG: Cr: Er laser with an intracavity polarizer," *IEEE J. Quantum Electron.*, vol. **27**, pp. 274-276, 1991.

[53] K. L. Vodop'yanov, L. A. Kulevskii, P. P. Pashinin, and A. M. Prokhorov, "Water and ethanol as bleacheable absorbers of radiation in yttrium-erbium-aluminum garnet laser ($\lambda = 2.94$ μm)," *Sov. Phys. - JETP*, **55**, 1049-1051 (1982).

[54] K. L. Vodop'yanov, A. V. Lukashev, and C. C. Phillips, "Nano- and picosecond 3 μm Er: YSGG laser using InAs as passive Q-switchers and mode lockers," *Opt. Commun.*, **95**, 87-91 (1993).

[55] A. Högele, G. Hörbe, H. Lubatschowski, H. Welling, and W. Ertmer, "2.70 μm CrEr: YSGG laser with high output energy and FTIR-Q-switch," *Opt. Commun.*, **125**, 90-94 (1996).

[56] A. Högele, C. Ziolek, H. Lubatschowski, S. Lohmann, H. Welling, A. Olmes, and W. Ertmer, "FTIR-Q-switched 3 μm erbium lasers for applications in laser surgery," *Laser und Optoelektronik*, **29**, April, 1997.

[57] H. J. Eichler, B. Liu, M. Kayser, and S. I. Khomenko, "Er: YAG-laser at 2.94 μm Q-switched by a FTIR-shutter with silicon output coupler and polarizers," *Opt. Materials,* **5**, 259-265 (1996).

[58] K. L. Vodop'yanov, V. I. Zhekov, L. Kulevskii, V. A. Lobachev, T. M. Murina, and A. M. Prokhorov, *Laser with Yttrium-Erbium-Aluminum Garnet*, T. M. Murina, Ed., in *Proc. IOFAN*, Moscow: Nauka, 1989, vol. 19, pp. 69-111 (in Russian).

[59] E. V. Zharikov, V. I. Zhekov, T. M. Murina, V. V. Osiko, M. I. Timoshechkin, I. A. Shcherbakov, "Cross-section of the $^4I_{11/2} \rightarrow {}^4I_{13/2}$ laser transition in Er^{3+} ions in yttrium-erbium-aluminum garnet crystals," *Sov. J. Quantum Electron.*, **7**, 117-119 (1977).

[60] V. I. Zhekov, T. M. Murina, A. M. Prokhorov, M. I. Studenikin, S. Georgescu, A. Lupei, V. Lupei, "Nonradiative transfer of excitation energy in crystals with the interaction of three optically active centers," *JETP Lett.*, **52**, 670-674 (1991).

[61] J. J. Degnan, "Theory of the optimally coupled Q-switched laser," *IEEE J. Quantum Electron.*, **25**, 214-220 (1989).

[62] Kh. H. Bagdasarov, V. I. Zhekov, V. A. Lobachev, A. A. Manenkov, T. M. Murina, A. M. Prokhorov, M. I. Studenikin, E. A. Fedorov, "Laser with yttrium-erbium-aluminum garnet," in *Proc. IOFAN*, Moscow: Nauka, 1989, **19**, 5-68 (1989).

[63] S. Georgescu, C. Hapenciuc, and C. Florea, "On the intrinsic oscillation threshold of 3-μm erbium lasers," *Internat Conf. ROMOPTO 2000*, Bucharest, sept. 2000 (will be published in Proc. SPIE).

[64] S. Georgescu, V. Lupei, A. Petraru, C. Hapenciuc, C. Florea, C. Naud, and C. Porte, "Excited-State-Absorption in low concentrated Er: YAG crystals for pulsed and cw pumping," (*to be published in J. Lumin.*)

[65] B. Majaron, T. Rupnic, and M. Luka, "Temperature and gain dynamics in flash-lamp pumped Er: YAG," *IEEE J. Quantum Electron.*, **32**, 1636-1644 (1996).

Şerban Georgescu,
National Institute for Laser, Plasma and Radiation Physics,
111 Atomistilor Str., C. P. MG-36, R-76900, Bucharest, Romania.
Phone: 423 1228, Fax: 423 1791, e-mail: joe@pluto.infim.ro